Catalysis

DOI: 10.1002/anie.201109257

BCN Graphene as Efficient Metal-Free Electrocatalyst for the Oxygen Reduction Reaction**

*Shuangyin Wang, Lipeng Zhang, Zhenhai Xia, Ajit Roy, Dong Wook Chang, Jong-Beom Baek, and Liming Dai**

The cathodic oxygen reduction reaction (ORR) is an important process in fuel cells and metal–air batteries.[1–3] Although Pt-based electrocatalysts have been commonly used in commercial fuel cells owing to their relatively low overpotential and high current density, they still suffer from serious intermediate tolerance, anode crossover, sluggish kinetics, and poor stability in an electrochemical environment. This, together with the high cost of Pt and its limited nature reserves, has prompted the extensive search for alternative low-cost and high-performance ORR electrocatalysts. In this context, carbon-based metal-free ORR electrocatalysts have generated a great deal of interest owing to their low-cost, high electrocatalytic activity and selectivity, and excellent durability.[4–9] Of particular interest, we have previously prepared vertically aligned nitrogen-doped carbon nanotubes (VA-NCNTs) as ORR electrocatalysts, which are free from anode crossover and CO poisoning and show a threefold higher catalytic activity and better durability than the commercial Pt/C catalyst.[4] Quantum mechanics calculations[4] indicate that the enhanced catalytic activity of VA-NCNTs toward ORR can be attributed to the electron-accepting ability of the nitrogen species, which creates net positive charges on the CNT surface to enhance oxygen adsorption and to readily attract electrons from the anode for facilitating the ORR. Uncovering this new ORR mechanism in nitrogen-doped carbon nanotube electrodes is significant as the same principle could be applied to the development of various other metal-free efficient ORR catalysts for fuel-cell applications and even beyond fuel cells. Indeed, recent intensive research efforts in developing metal-free ORR electrocatalysts have led to a large variety of carbon-based metal-free ORR electrocatalysts, including heteroatom (N, B, or P)-doped carbon nanotubes, graphene, and graphite.[4–14] More recently, we have successfully synthesized vertically aligned carbon nanotubes co-doped with N and B (VA-BCN) and demonstrated a significantly improved electrocatalytic activity toward the ORR, with respect to CNTs doped with either N or B, only due to a synergetic effect arising from the N and B co-doping.[15] However, most of the reported carbon-based ORR electrocatalysts (particularly, heteroatom-doped nanotubes and graphene) were produced by chemical vapor-deposition (CVD) processes involving vacuum-based elaborate and careful fabrication, which are often too tedious and too expensive for mass production. As demonstrated in this study, therefore, it is of great importance to develop a facile approach to BCN graphene as low-cost and efficient ORR electrocatalysts. The recent availability of solution-exfoliated graphite oxide (GO)[16] allows the mass production of graphene and derivatives by conventional physicochemical treatments of GO.

Herein, we have developed a facile approach to metal-free BCN graphene of tunable B/N co-doping levels as efficient ORR electrocatalysts simply by thermal annealing GO in the presence of boric acid and ammonia. The resultant BCN graphene was shown to have superior electrocatalytic activities to the commercial Pt/C electrocatalyst (C2-20, 20% platinum on Vulcan XC-72R; E-TEK). First-principles calculations were performed to explain the high catalytic capability of the BCN graphene. This newly developed method can thus provide simple but efficient and versatile approaches to low-cost mass production of BCN graphene as efficient metal-free ORR electrocatalysts for fuel cells and other applications.

Figure 1 shows XPS survey spectra for three BCN graphene samples of different chemical compositions, along with the mixture of GO and boric acid (B-GO) starting material as reference. Comparing with the B-GO starting mixture, the salient feature for BCN graphene samples is the appearance of a pronounced XPS N1s peak, indicating the incorporation of N in addition to B into GO by thermal annealing in the presence of boric acid and ammonia. Like VA-BCN nanotubes,[15] the presence of a O1s peak in the BCN graphene samples is due to the incorporation of

[*] Dr. S. Wang, Prof. L. Dai
Center of Advanced Science and Engineering for Carbon (Case4-Carbon), Department of Macromolecular Science and Engineering, Case Western Reserve University
10900 Euclid Avenue, Cleveland, OH 44106 (USA)
E-mail: liming.dai@case.edu
L. Zhang
Department of Mechanical Engineering, The University of Akron
Akron, OH44325 (USA)
Prof. Z. Xia
Department of Materials Science and Engineering, Department of Chemistry, University of North Texas (USA)
Dr. A. Roy
Thermal Science and Materials Branch, Materials & Manufacturing Directorate, Air Force Research Laboratory (USA)
Dr. D. W. Chang, Prof. J.-B. Baek
Interdisciplinary School of Green Energy, Ulsan National Institute of Science and Technology (UNIST) (South Korea)

[**] This work was supported financially by AFOSR (FA 9550-10-1-0546), FOSR MURIA (FA9550-12-1-0037), AFRL (FA8650-07-D-5800) through UTC (11-S587-100-01-C1), the WCU Project through UNIST, and US AFOSR-Korea NBIT.

Supporting information for this article is available on the WWW under http://dx.doi.org/10.1002/anie.201109257.

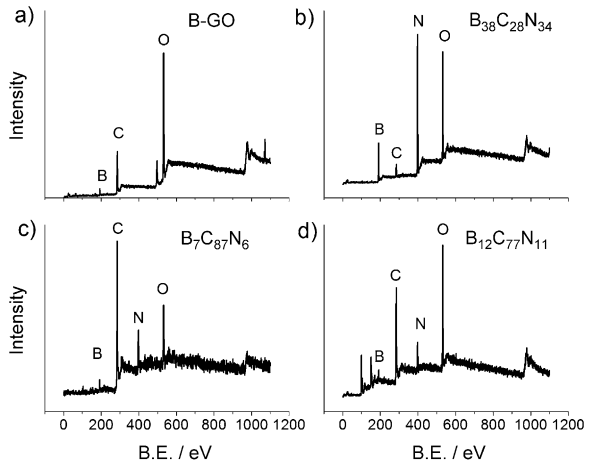

Figure 1. XPS survey spectra for a) a boric acid–graphene oxide mixture, and b–d) BCN graphene samples with annealing times of b) 2 h, c) 0.5 h, and d) 1 h at 1000 °C.

around 190 eV, indicating that B atoms have been successfully incorporated into the graphene lattice network. The CN, CB, and BN chemical bonds have also been observed in the corresponding FTIR spectrum shown in Figure 2c. As seen from Raman spectra in Figure 2d, a D band located around 1342 cm^{-1} and a G band around 1570 cm^{-1} were observed. The G band arises from the bond stretching of all sp^2-bonded pairs, including C–C, B–C, N–C, and B–N, while the D band is associated with the sp^3 defect sites. The higher-order peak appeared at 2680 cm^{-1} and a small broad peak at 2910 cm^{-1} can be assigned to a combination of D + D and D + G bands. Although there is no significant change in the position of D and G bands, BCN graphene shows a different I_D/I_G value from that of graphene oxide and N-doped graphene. As can be seen in Figure 2d, the intensity ratio of I_D/I_G increased from GO to N-doped graphene owing to the introduction of defects by N-doping. Upon co-doping with B and N, the intensity ratio of I_D/I_G increased further.

The proven synergetic effect associated with the N and B co-doping,[15] together with the superb thermal stability (Supporting Information, Figure S1) and porosity (Supporting Information, Figure S2), makes the BCN graphene attractive for metal-free ORR electrocatalysts, particularly at elevated temperatures. As shown in Figure 3a, a substantial reduction process occurred at about −0.28 V in the presence of oxygen, whereas no obvious response was observed at the same potential range under nitrogen. The linear-sweep voltammetry (LSV) curves given in Figure 3b clearly show that the ORR activity is very low for $B_{38}C_{28}N_{34}$, which is probably due to its low conductivity associated with the low carbon content (see below). In contrast, $B_{12}C_{77}N_{11}$ shows an onset potential close to that of the commercial Pt/C catalyst, indicating an excellent ORR catalytic activity induced by the synergetic effect through co-doping with N and B.[15] The electron transfer number *n* of ORR on this BCN graphene electrocatalyst is close to 4, as determined by the rotating ring disk electrode (RRDE) data shown in the Supporting Information, Figure S3.

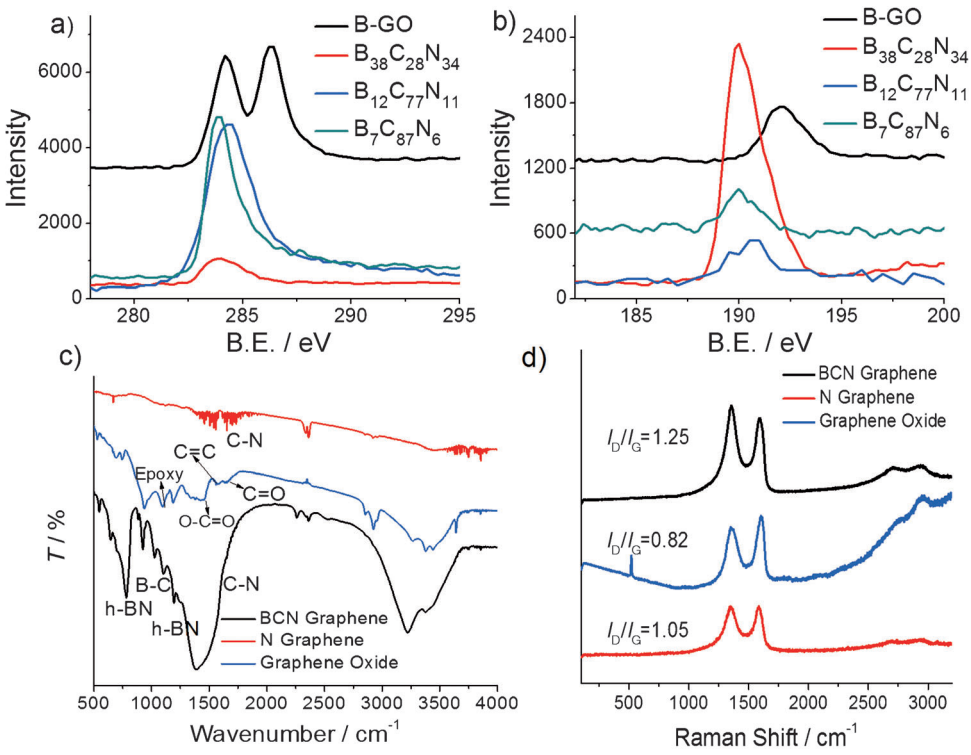

Figure 2. High-resolution a) XPS C1s, b) XPS B1s, c) FTIR, and d) Raman spectra of BCN graphene in comparison with N-doped graphene, graphene oxide, or boric acid and graphene oxide mixtures.

physicochemically adsorbed oxygen, suggesting an additional advantage as the ORR electrode.[15]

As oxygen-containing groups in GO were reduced by thermal treatment, the high-resolution XPS C1s spectra given in Figure 2a clearly show an almost total loss of the oxygen component above 286 eV, while the carbon peak at 284.5 eV becomes more asymmetric. Figure 2b shows the corresponding high-resolution XPS B1s spectra. For the mixture of GO and boric acid, the binding energy of B1s at around 192 eV is attributable to the boron oxide. For the BCN graphene samples, however, the binding energy of B1s shifted down to

In fuel cells and air batteries, the oxygen cathode should have a high working potential to ensure a reasonable reaction rate and sufficiently high energy conversion efficiency. Therefore, it is important to compare the potential of oxygen reduction for different catalysts. The so-called half-wave potential, a potential at which the current is a half of the

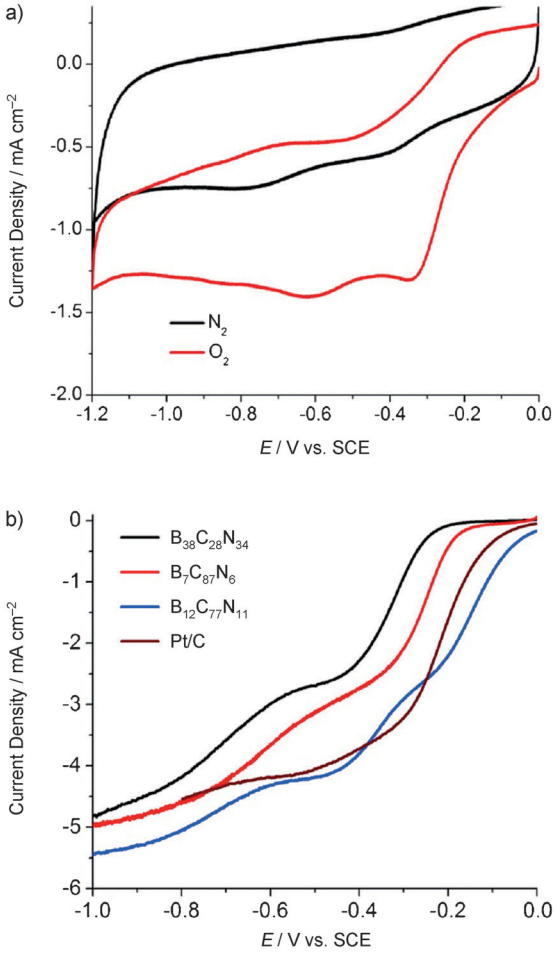

Figure 3. a) Cyclic voltammetry (CV) curves of ORR on BCN ($B_{12}C_{77}N_{11}$) graphene in nitrogen- and oxygen-saturated 0.1 M KOH solutions at a scan rate of 50 mV s^{-1}. b) LSV curves of ORR on BCN graphene with different compositions in oxygen-saturated 0.1 M KOH solution at 10 mV s^{-1} and compared with the commerical Pt/C electrocatalyst.

limiting current in a LSV curve, has been conveniently used for this purpose. It is interesting to see from Figure 3b that the half-wave potential of the $B_{12}C_{77}N_{11}$ electrode for ORR in 0.1M KOH solution was at around −0.25 V, which is close to that of the Pt/C but much more positive than those of other BCN graphene electrodes. Furthermore, the current density of ORR on $B_{12}C_{77}N_{11}$ within almost the whole potential range covered in this study is higher than that of the other BCN and Pt/C electrodes. The above results from these not-yet optimized BCN graphene electrodes clearly indicate that the controlled doping of graphene with B and N could significantly improve the electrocatalytic activity toward ORR.

The electrocatalytic activity of the BCN graphene was also studied theoretically by density functional (DFT) calculations with Gaussian 03 (Revision E.01; Gaussian, Inc., Wallingford, CT, 2004). The details of this calculation are described elsewhere.[17] As shown in Figure 4, we constructed three BCN graphene models, $B_7C_{87}N_6H_{26}$, $B_{12}C_{77}N_{11}H_{26}$, and $B_{38}C_{28}N_{34}H_{26}$, which correspond to the experimental samples. For comparison, pure graphene, $C_{100}H_{26}$, with the same size as

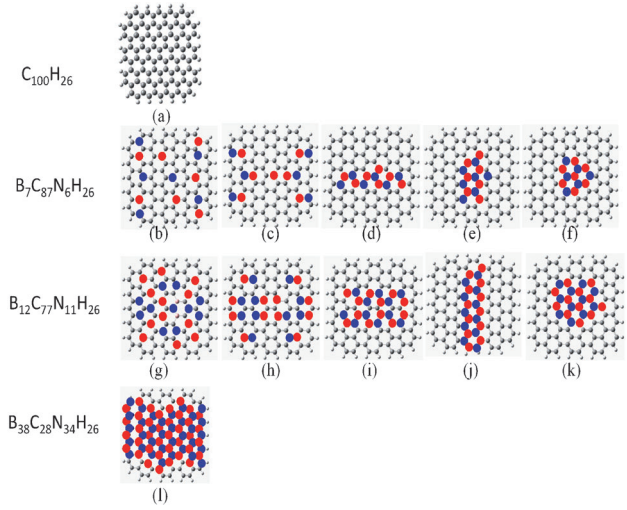

Figure 4. BCN graphene models: a) pure graphene ($C_{100}H_{26}$), b)–f) $B_7C_{87}N_6H_{26}$, g)–k) $B_{12}C_{77}N_{11}H_{26}$, and l) $B_{38}C_{28}N_{34}H_{26}$. C gray, H white, B pink, N blue.

those BCN graphene samples, was also constructed. As the distributions of boron and nitrogen atoms on graphene are unspecified, we constructed five possible structures with the same composition for $B_7C_{87}N_6H_{26}$ and $B_{12}C_{77}N_{11}H_{26}$. As mentioned earlier, $B_{38}C_{28}N_{34}$ is not ideal for the ORR application owing to its low conductivity associated with the large BN cluster (Figure 4l). In these structures, the B and N distribute either randomly without any BN bonds or in small BN clusters, or single relatively large BN cluster, as shown in Figure 4b–k.

We first calculated the highest-occupied molecular orbital (HOMO) and lowest-unoccupied molecular orbital (LUMO) energy separation of the pure and BCN graphene structures. A small HOMO–LUMO gap implies low kinetic stability and high chemical reactivity because the smaller energy gap means that the state of the graphene is energetically favorable to add electrons to a high-lying LUMO and to extract electrons from a low-lying HOMO, and thus the facile formation of activated complexes for any potential reaction.[18] Table 1 lists the value of HOMO–LUMO energy gap for these graphene structures. Compared to pure graphene, the substitution of C by B and N leads to a smaller energy gap. However, overdoping of B and N, as is the case of

Table 1: HOMO-LOMO energy gap, spin density, and charge density of pure and BN graphene structures.

Structures	Energy gap [eV]	Maximum spin density (Spin density > 0.15)[b]	Maximum charge density (Charge density > 0.15)[b]
$C_{100}H_{26}$	0.80	0	0.19 (4.0%)
$B_7C_{87}N_6H_{26}$[a]	0.79	0.33 (3.6%)	0.38 (10.8%)
$B_{12}C_{77}N_{11}H_{26}$[a]	0.71	0.36 (2.8%)	0.56 (21.6%)
$B_{38}C_{28}N_{34}H_{26}$	1.23	0	0.34 (37.0%)

[a] Average values of five structures. [b] The number (percentage) in parenthesis represents the number of the atoms with a spin or charge density larger than 0.15, divided by the total number of atoms in the graphene, excluding the H atoms.

$B_{38}C_{28}N_{34}H_{26}$, results in a significant increase in the energy gap. As a result, $B_{38}C_{28}N_{34}H_{26}$ has the highest energy gap, which is almost two times as high as that of others. As the conductivity of the materials is inversely proportional to the band gap, the conductivity of $B_{38}C_{28}N_{34}H_{26}$ is significantly reduced. This could greatly affect its electron transfer and thus catalytic capability. Among all these structures, $B_{12}C_{77}N_{11}H_{26}$ has the lowest energy gap, suggesting that $B_{12}C_{77}N_{11}H_{26}$ should have the highest chemical reactivity or the best catalytic performance. These theoretical predictions are consistent with the experimental results discussed above (Supporting Information, Figure S4).

The atomic spin and charge densities determine the catalytic capability of materials for ORR.[4,17] Our previous work shows that the carbon atoms with positive spin or charge density larger than 0.15 are most likely to serve as catalytic active sites.[19] Thus, the number of atoms with large positive spin or charge density is another measure of its catalytic capability. The atomic spin density and charge density were calculated for these BCN graphene model structures (Supporting Information, Figure S5), and the largest spin and charge densities, together with the percentage of atoms with large spin or charge density, are also listed in Table 1. The pure ($C_{100}H_{26}$) and highly doped ($B_{38}C_{28}N_{34}H_{26}$) graphene do not have spin density at all. Although the highly doped graphene contains the most atoms (37%) with large charge density (>0.15), all these atoms are boron distributed in BN phase (Supporting Information, Figure S5d). Because the BN cluster is insulating, electron transfer in this graphene sample can be difficult during ORR. In contrast, $B_7C_{87}N_6H_{26}$ and $B_{12}C_{77}N_{11}H_{26}$ have many more carbon atoms with relatively high spin density and charge density compared to the pure graphene, thus providing more active sites to catalyze ORR. Of these two structures, the number of possible catalytic sites in $B_{12}C_{77}N_{11}H_{26}$ is twice that in $B_7C_{87}N_6H_{26}$. This explains well why the $B_{12}C_{77}N_{11}H_{26}$ model structure and $B_{12}C_{77}N_{11}$ graphene sample show the best ORR catalytic performance.

The BCN electrode was further subjected to testing the electrochemical stability, possible methanol crossover, and carbon monoxide (CO) poison effects. The current–time (*i-t*) chronoamperometric responses for ORR at the BCN graphene ($B_{12}C_{77}N_{11}$) and Pt/C electrodes are given in the Supporting Information, Figure S6, and show a sharp decrease in current upon the addition of 3.0 M methanol for the Pt/C electrode (Supporting Information, Figure S6a). In contrast, the amperometric response from the BCN graphene electrode remained almost uncharged even after the addition of methanol, indicating a higher selectivity toward ORR and better methanol tolerance than the commercial Pt/C electrocatalyst. As shown in Figure S6b, the BCN electrode was insensitive to CO whereas the Pt/C electrode was rapidly poisoned under the same condition. Figure S6c shows the durability test for the BCN graphene electrode. As can be seen, the continuous oxygen reduction reaction (ca. 40000 s) at −0.2 V (vs. SCE) caused only a slight loss (10%) of the current density before leveling off. In contrast, the corresponding current loss on Pt/C electrode under the same condition was as high as about 55%. These results clearly indicate that the catalytic active sites on the BCN graphene are much more stable than those on the commercial Pt/C electrode.

In summary, we have successfully developed a facile low-cost approach to mass production of BCN graphene with tunable N-/B-doping levels simply by thermal annealing graphene oxide in the presence of boric acid under ammonia atmosphere. The resultant metal-free BCN graphene samples were demonstrated to show ORR electrocatalytic activities even better than the commercial Pt/C electrocatalyst (C2-20, 20% platinum on Vulcan XC-72R; E-TEK). In a good agreement with the experimental observations, the first-principles calculations revealed a doping-level-dependent energy bandgap, spin density, and charge density. BCN graphene with a modest N- and B-doping level was demonstrated to show the best ORR electrocatalytic activity, fuel selectivity, and long-term durability, along with an excellent thermal stability and porosity. The thermal annealing graphene oxide in the presence of boric acid under ammonia can thus provide simple but efficient and versatile approaches to low-cost mass production of BCN graphene as efficient metal-free ORR electrocatalysts for fuel cells and many other applications, such as metal–air batteries.

Received: December 30, 2011
Published online: March 16, 2012

Keywords: B/N doping · electrocatalysis · fuel cells · graphene · oxygen reduction

[1] M. Shao, K. Sasaki, R. Adzic, *J. Am. Chem. Soc.* **2006**, *128*, 3526.
[2] C. Wang, H. Daimon, T. Onodera, T. Koda, S. Sun, *Angew. Chem.* **2008**, *120*, 3644; *Angew. Chem. Int. Ed.* **2008**, *47*, 3588.
[3] V. Stamenkovic, B. Fowler, B. Mun, G. Wang, P. Ross, C. Lucas, N. Markovic, *Science* **2007**, *315*, 493.
[4] K. Gong, F. Du, Z. Xia, M. Durstock, L. Dai, *Science* **2009**, *323*, 760.
[5] R. Liu, D. Wu, X. Feng, K. Mullen, *Angew. Chem.* **2010**, *122*, 2619; *Angew. Chem. Int. Ed.* **2010**, *49*, 2565.
[6] L. Qu, Y. Liu, J. Baek, L. Dai, *ACS Nano* **2010**, *4*, 1321.
[7] Y. Shao, S. Zhang, M. Engelhard, G. Li, G. Shao, Y. Wang, J. Liu, I. Aksay, Y. Lin, *J. Mater. Chem.* **2010**, *20*, 7491.
[8] D. Yu, Q. Zhang, L. Dai, *J. Am. Chem. Soc.* **2010**, *132*, 15127.
[9] S. B. Yang, X. L. Feng, X. C. Wang, K. Mullen, *Angew. Chem.* **2011**, *123*, 5451; *Angew. Chem. Int. Ed.* **2011**, *50*, 5339.
[10] S. Wang, D. Yu, L. Dai, *J. Am. Chem. Soc.* **2011**, *133*, 5182.
[11] L. Yang, S. Jiang, Y. Zhao, L. Zhu, S. Chen, X. Wang, Q. Wu, J. Ma, Y. Ma, Z. Hu, *Angew. Chem.* **2011**, *123*, 7270; *Angew. Chem. Int. Ed.* **2011**, *50*, 7132.
[12] D. Yu, E. Nagelli, F. Du, L. Dai, *J. Phys. Chem. Lett.* **2010**, *1*, 2165.
[13] X. Wang, J. Lee, Q. Zhu, J. Liu, Y. Wang, S. Dai, *Chem. Mater.* **2010**, *22*, 2178.
[14] Z. Liu, F. Peng, H. Wang, H. Yu, W. Zheng, J. Yang, *Angew. Chem.* **2011**, *123*, 3315; *Angew. Chem. Int. Ed.* **2011**, *50*, 3257.
[15] S. Wang, E. Iyyamperumal, A. Roy, Y. Xue, D. Yu, L. Dai, *Angew. Chem.* **2011**, *123*, 11960; *Angew. Chem. Int. Ed.* **2011**, *50*, 11756, and references therein.
[16] W. Hummers, R. Offeman, *J. Am. Chem. Soc.* **1958**, *80*, 1339.
[17] L. Zhang, Z. Xia, *J. Phys. Chem. C* **2011**, *115*, 11170.
[18] J. Aihara, *J. Phys. Chem. A* **1999**, *103*, 7487.
[19] L. Zhang, J. Niu, L. Dai, Z. Xia, *Langmuir* **2011**, submitted.

